THE CANNERO CASTLE (ITALY): DEVELOPMENT OF RADIOCARBON DATING METHODOLOGIES IN THE FRAMEWORK OF THE LAYERED DOUBLE HYDROXIDE MORTARS

Giulia Ricci[1,2]* • Michele Secco[2,3] • Fabio Marzaioli[4] • Filippo Terrasi[4] •
Isabella Passariello[4] • Anna Addis[5] • Paolo Lampugnani[6] • Gilberto Artioli[1,2]

[1]Department of Geosciences, University of Padova, Italy
[2]Inter-Departmental Research Center for the Study of Cement Materials and Hydraulic Binders (CIRCe), University of Padova, Italy
[3]Department of Cultural Heritage (DBC), University of Padova, Italy
[4]Centre for Isotopic Research on Cultural and Environmental Heritage (CIRCE), INNOVA SCaRL and Department of Mathematics and Physics, Campania University "Luigi Vanvitelli", Caserta, Italy
[5]Bruker Italia S.r.l., Daltonics Division, Via Cluentina, 26/R (62100), Macerata, Italy
[6]Pandora Archeologia, Veruno, Italy

ABSTRACT. The mortar samples of the Castle of Cannero (Lake Maggiore, Italy) have been characterized and radiocarbon (^{14}C) dated. The presence of LDH phases was identified. The hydraulic reaction was evaluated by a multi-analytical approach. Careful extraction, preparation and purification of the binder fraction have been performed. Contaminations due to LDH phases have been removed allowing reliable absolute dating of the structures.

Non-hydraulic lime-based mortars represent only part of the binding materials found in archaeological and historical structures, and a new challenge is the application of ^{14}C dating techniques on mortars that feature hydraulic reactions. This research work aims at ^{14}C dating a series of Mg-rich hydraulic mortars from the Castle of Cannero (Lake Maggiore, Italy), from which both charcoals and mortar samples were collected. A multi-analytical approach employing X-ray powder diffraction (XRPD), optical microscopy (OM), and scanning electron microscopy/energy-dispersive microanalysis (SEM-EDS) was adopted in order to carefully characterize the samples. A wet gravimetric separation for the extraction of the fine fraction mainly composed by the mortar binder was carried out and the binder fraction was characterized by XRPD in order to investigate the presence of contaminants. The binding fractions are characterized by the widespread occurrence of hydrotalcite-type minerals, considered contaminants in ^{14}C dating of mortars because of their capability to exchange carbonate anions even after the hardening process. A further purification treatment by thermal decomposition was performed before ^{14}C dating by AMS. The obtained dates were consistent with archaeological expectations, confirming the potential of the developed purification methodology for hydraulic mortars dating.

KEYWORDS: binder separation, ^{14}C mortar dating, hydrocalumite and hydrotalcite, purification treatment, thermal decomposition.

INTRODUCTION

The principle of the radiocarbon (^{14}C) dating method of lime mortars has been discussed and applied since the 1960s, and in the case of lime-based mortars with a one-step carbonation history, new and modified protocols are applied in order to provide plausible dates relative to the time of setting and hardening of the binder (Delibrias and Labeyrie 1964; Heinemeier et al. 2010; Van Strydonck 2016; Hajdas et al. 2017). However, such an ideal situation is hardly encountered in practical cases, where ^{14}C dating of the carbonated binder is variously affected mainly by: (i) geologic or fossil carbonate, which could affect the dating incorporating dead carbon and overestimating the age; (ii) secondary alteration processes, lime lumps, delayed hydraulic reactions and formation of new phases containing carbonate occurring over a relatively long period, could be responsible of an under estimation of the age (Lindroos et al. 2007; Artioli 2010; Miriello et al. 2010; Michalska and Czernik 2015; Ponce-Antón et al. 2018).

---

*Corresponding author. Email: giulia.ricci@unipd.it.

Moreover, the situation is further complicated if Mg-rich phases are present, either derived from the aerial reaction of lime binders obtained from the calcination of dolomitic carbonate compounds, or after pozzolanic reaction processes between the lime binder and reactive silicates. The different kinetics of carbonation between the Ca-phases (lime, portlandite) and the Mg-phases (periclase, brucite) induce different setting times, also enhancing the delayed formation of carbonate-containing double layered hydroxides (LDH) of the hydrotalcite-type, with severe effects on the radiocarbon dating of the structures (Artioli et al. 2017; Ponce-Antón et al. 2018).

LDHs are layered hydroxides characterized by a flexible layered structure prone to dynamic exchanges of carbonate anions derived from atmospheric CO_2 (Ishihara et al. 2013; Conterosito et al. 2018). LDHs usually formed during delayed hydraulic reactions of mortars are: (Mg, Al) LDHs of the hydrotalcite group or (Ca, Al) LDHs of the hydrocalumite group. Their crystal-chemical characteristics depend on the composition of the raw materials used, and the occurrence in the mortar mixes of Mg, Al-containing materials as natural clays or pyroclastic products can trigger the stabilization of compounds of the hydrotalcite group. Hydrotalcite $[Mg_6Al_2(CO_3)(OH)_{16} \cdot 4(H_2O)]$ is characterized by brucite-like layers (where Al^{3+} ions are combined with Mg^{2+} ions from MgO in octahedral sites) alternated by water molecules and anions-containing layers. Anions such as CO_3^{2-} stabilize the positive charge and recent studies demonstrated that carbonate anions within the interlayers of LDHs undergo dynamic exchanges with atmospheric CO_2 even under ambient conditions. This high capability in capturing large anions is a characteristic of the structure and chemical properties of LDHs minerals (Ishihara et al. 2013; Artioli et al. 2017; Mishra et al. 2018; Ponce-Antón et al. 2018). As reported in literature, LDH phases have been observed as products of pozzolanic reaction between lime and clays in ancient mortars, in modern pozzolanic cements, as well as in dolomitic lime mortars (Brandon et al. 2014; Artioli et al. 2017; Ponce-Antón et al. 2018; Secco et al. 2018).

The complexity of ancient mortar systems requires the development of effective methods both for the characterization and the separation of the binder fractions for mortar dating. In this framework, sample preparation procedures have been implemented over time in order to isolate the pure carbonate binder fraction removing any other contaminant, but the issue is still not completely resolved (Sonninen and Jungner 2001; Nawrocka et al. 2005; Lindroos et al. 2007; Marzaioli et al. 2014; Addis et al. 2019).

Our approach in studying and dating historical mortars consists of combining a careful extraction and preparation of the fine binder fraction with a full mineralogical characterization of both bulk and extracted samples. The characterization is crucial: it provides useful data that helps to determine whether the sample is suitable for dating and which criteria are needed for a more efficient separation of the carbonate fraction of interest. Moreover, in order to separate the binder from other contaminant sources, a multistep purification protocol based on size selection by wet sieving has been developed (Addis et al. 2019). Nevertheless, if the mortar has been affected by hydraulic reaction processes, LDH phases may be present in the isolated binder fraction prepared for the dating process. LDHs can exchange carbonate anions with the atmosphere well after the laying of the mortar and during the life of the building, compromising the success of the dating by introducing younger CO_2 into the system. Hence, it is clear that detecting and eliminating these phases are essential operations. X-ray powder diffraction is a powerful technique able to detect LDHs

(Roelofs et al. 2002; Tian et al. 2014). In the present work lime-based mortars from Castle of Cannero presenting hydraulic reaction have been studied and dated even if hydrotalcite-like compounds were detected. The Castle of Cannero (Italy) has a complex construction history between the XIV and XVI centuries, and during the archaeological excavation and investigation (in 2016–2017), archaeologists had difficulties in discriminating the different construction phases.

The multi-analytical approach adopted in this research exploited the potential of X-ray powder diffraction (XRPD), optical microscopy (OM) and scanning electron microscopy coupled with energy-dispersive spectroscopy (SEM-EDS) in order to carefully characterize the mortars. Furthermore, a wet gravimetric separation for the extraction of the fine fraction (SG) mainly composed of the mortar binder was carried out and the SG was characterized by XRPD to investigate the presence of contaminants. Before radiocarbon dating by accelerator mass spectrometry (AMS), the SGs were further purified by thermal treatment under vacuum at 550°C in order to eliminate the carbonate fraction of LDHs or other Mg-compounds detected in the SGs. The archaeometric study was able to give a more complete construction sequence to corroborate the data deriving from excavation activities and historical research.

HISTORICAL BACKGROUND

Borromeo's Castle is located in a modest rocky spur emerging from the Lake Maggiore, 300 m from the coast, between the cities of Cannero and Cannobio, in the northwest Italian region Piedmont. Historical sources (Lose and Lose 1818; Bottacchi and Mancini 2000; Pisoni 2003; Frigerio and Pisoni 2006), report that the Mazzardi family, called "Mazzarditi", settled on the island and built the first fortress for territorial defenses in the early 1400s. The Mazzarditi had the coast and the nearby cities' military control. Upon request of the inhabitants of the coast, an armed group sent by the Duke of Milan, Filippo Maria Visconti, conquered and destroyed the castle in 1414–1415. Thirty years later, in 1441, the Duke of Milan ceded the castle's ruins to Vitaliano I Borromeo, son of Filippo I Borromeo and Franceschina Visconti. Since that time, the castle was owned by the Borromeo Family. The current complex, called Rocca Vitaliana, was built during a narrow time span (between 1519 and 1521) by Ludovico Borromeo with the purpose of military and commercial control, as well as a residence for the family itself. Until the 1700s it was used by the family but then it was abandoned and left as a shelter for fishermen, until recent years, when a recovery project began under the supervision of the *Soprintendenza Archeologia, Belle Arti e Paesaggio* of the provinces of Biella, Novara, Verbano-Cusio-Ossola, and Vercelli. During the excavation in 2016–2017, archaeological investigations were not completely able to discriminate different construction phases at the complex. The main purpose was to investigate and distinguish the original phases of the architectural structures belonging to the first fortress of the 15th century to that one built by Borromeo in the 16th century. For this endeavor, archaeometric investigations were requested and performed.

MATERIALS AND METHODS

Sample Descriptions

Seventeen samples (14 mortar and 3 charcoal samples [CM]) were collected in 3 sampling areas from the architectural structures (Figure 1). Within the residential part of the complex (area I), in which the ground floor of the tower on the west side and the first room of the residential
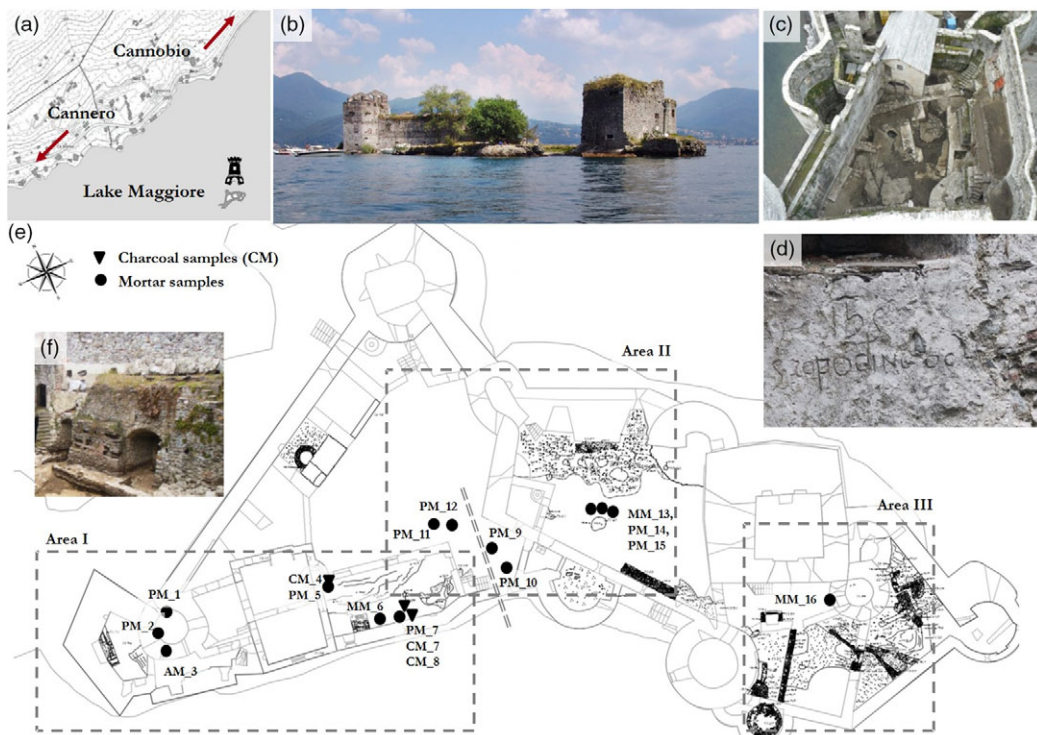
Figure 1   (a) Map of Lake Maggiore showing the location of the castle and the cities of Cannero and Cannobio; (b) pictures of the Castle of Cannero's ruins; (c) top view of the main court; (d) *graffito* inscription reporting the year of the construction (1522) on a wall in the southern tower; (e) plan of the complex showing the three sampling areas and the collected samples; (f) structures in the main court of the complex.

building were identified, 9 samples were taken: 6 mortars and 3 charcoal fragments embedded in the mortars (CM_4 was collected from the mortar sample PM_5, whereas CM_7 and CM_8 were collected from the sample PM_7 which was part of the hearth at the ground floor). In the area II, including the large west court and the main court of the complex, 7 mortars were taken. Here, the archaeological excavation was not able to chronologically constrain the age of the different structures, as no evidence was found in order to attribute those structures to the first fortress (15th century) or to the Borromeo one (16th century). Finally, a sample of mortar was taken in the tower wall of the area III, related to a rectangular court nearby to the southern tower, where a *graffito* inscription reports the year of the structure construction (1522 AD) (Figure 1d).

Analytical Approach

The analytical process was divided into several phases: (a) a chemical-mineralogical characterization of the mortars in order to assess materials' properties and the presence of potential dating contaminants, and to develop a more efficient separation procedure of the binder fraction; (b) a series of purification procedures of the binder by wet gravimetric separation; (c) a characterization of the extracted fine powder in order to evaluate the effectiveness of the purification; (d) a sample treatment for the elimination of possible contaminants; (e) a final acid digestion, graphitization and radiocarbon dating of the

purified fraction. Characterization and purification procedures were performed at the CIRCe Centre in Padua (Italy), graphitization and AMS measurements were carried out at CIRCE Centre in Caserta (Italy).

Mortar Characterization

The 14 mortar samples were characterized according to a multi-analytical approach. Petrographic analyses were performed by OM on 30 μm thin-sections under parallel and crossed polars using a Nikon Eclipse ME600 microscope equipped with a Canon EOS 600D Digital single-lens reflex camera. The thin sections, covered with an ultrathin coating of graphite, were microstructurally and microchemically characterized through a CamScan MX2500 SEM equipped with a LaB_6 electron source and an EDS used to collect elemental microanalyses (system resolution of 126.8 eV for 5.9 eV) through the SEMQuant Phizaf software, giving valuable information on the mineral phases and binder composition. Mineralogical quantitative phase analyses (QPAs) were performed by XRPD on fine sample powders obtained by micronization. The quantitative measurements are expressed in wt% ± (Rietveld error), which is the most quoted value used as the error related to phase abundance and represents the uncertainty in the mathematical fit between the observed and calculated patterns (Madsen and Scarlett 2008; Gualtieri et al. 2019). XRPD analyses were performed using a Malvern PANalytical X'Pert PRO diffractometer in Bragg-Brentano geometry, Co–Kα radiation, 40 kV and 40 mA, equipped with a real-time multiple strip (RTMS) detector (X'Celerator by Malvern Panalytical). Data acquisition was performed by operating a continuous scan in the range 3–85° 2θ, with a virtual step scan of 0.02° 2θ. Diffraction patterns were interpreted with X'Pert HighScore Plus 3.0 software by Malvern PANalytical, reconstructing mineral profiles of the compounds by comparison with ICDD and ICSD diffraction databases. QPAs were performed using the Rietveld method (Rietveld 1969) and refinements were accomplished using the TOPAS software (version 4.1) by Bruker AXS. The determination of both crystalline and amorphous content was calculated by means of the internal standard method with the addition of 20 wt% of zincite (ZnO) to the powders (Gualtieri 2000).

^{14}C Analyses

Eight mortar samples were selected according to their archaeological significance and ca. 30 g of manually disaggregated material for each sample were subjected to the separation protocol in order to extract the SGs from the other mortar components based on their grain sizes. The procedure consists in a sonication and wet gravimetric sedimentation in ultrapure decarbonated water for 24 hr, centrifugation and filtration of the fine fraction (Nonni et al. 2017; Addis et al. 2019). The obtained SGs were analyzed by XRPD in order to evaluate the presence of contaminants for the radiocarbon dating. Thermal treatment at 550°C for 30 min in vacuum condition was carried out on the SG fractions (over 30 mg for each sample) in order to break down the LDH structure. The outcome of the thermal treatment (OTT), i.e. released CO_2 of the LDHs, was collected and underwent to the graphitization process for AMS measurements. The selected temperature was chosen according to the thermal decomposition temperature of LDHs and carbonates. Decomposition of Ca-carbonate starts at around 650°C and ends at 800–850°C (Trindade et al. 2009). Mg-carbonates, main constituents of ancient magnesian mortars, decompose endothermically releasing water and CO_2 over a temperature range approximately between 220 and 550°C (Hollingbery and Hull 2010; Bhattacharjya et al. 2012). The transitions involved during LDH thermal decomposition have been widely investigated (Stanimirova et al. 1999; Roelofs et al. 2002; Pérez-Ramírez and Abelló 2006; Bhattacharjya et al. 2012;

Artioli et al. 2017), and, in general, a three-step mass loss behavior has been defined: dehydration (25–280°C), dehydroxylation (280–400°C) and anion expulsion (>400°C), leading to the progressive collapse of the double-layered structure. Furthermore, considering other LDH phases, the layered structure of hydrocalumite collapses when heated above 250°C, turns into an amorphous phase at 300°C, and it transforms into calcium oxide (CaO) and mayenite ($Ca_{12}Al_{14}O_{33}$) at 600–700°C (Vieille et al. 2003).

The residuals after thermal treatment (RaTT), were digested under vacuum by means of a complete orthophosphoric acid attack for 2 hr at 80°C (Marzaioli et al. 2011). The extracted CO_2 from both RaTT and OTT was reduced to graphite on iron powder catalyst according to the CIRCE sealed tube reaction protocol (Marzaioli et al. 2008). In details, IAEA C1 historical series (mass of carbon vs. apparent age) were used for background correction and IAEA C2 was used for normalization purposes (Marzaioli et al. 2011).

Charcoals found in mortars were mechanically extracted and pretreated, applying the conventional AAA (acid-alkali-acid) method in order to completely remove calcite contaminations (Berger 1992; Passariello et al. 2007). For these charcoals the time of the acid attack was increased by 2 hr.

[14]C isotopic ratios were measured according to Terrasi et al. (2008) and corrected for fractionation and blank, normalised by SRM 4990 C and R.C. ages were estimated (Stuiver and Polach 1977) and calibrated to absolute ages by means of OxCal 4.2 (Bronk Ramsey and Lee 2013) and IntCal13 calibration curve (Reimer et al. 2013).

RESULTS AND DISCUSSION

Mortar Characterization

Macroscopically, the samples appear to be highly cohesive with a light grey mass color. From a chemical-mineralogical point of view, the samples are similar, i.e. the constituents of the mortar are the same in terms of aggregates and type of binder used. OM and SEM observations showed that the samples are characterized by a heterogeneous matrix in which the aggregates are homogeneously distributed and constituted by isodiametric, angular and moderately selected clasts. Mineralogical and petrographic features of the inert fraction identified the presence of metamorphic lithologies as gneisses, schists, quartzites, and serpentinites associated with single crystals of quartz, feldspars, muscovite, and biotite. These characteristics can be attributed to a fluvial aggregate fraction with low erosion, consistent with local lithologies (Beneo 1961).

Two groups have been identified considering the binder-to-aggregate ratios calculated by OM observation of the thin sections and comparison with visual estimation charts (Figure 2). The first group (PM_1, PM_2, AM_3, PM_7, PM_9, MM_16) is characterized by a dark-colored matrix with 1:2 binder-to-aggregate ratio. The second one includes all samples taken in the sampling area II (except PM_9) and the MM_6 sample of the area I, and it clusters fatter mortars (1:1 binder-to-aggregate ratio) with lighter background colors and less sorted aggregates. The presence of lime lumps was identified in all the samples by OM observations (Figure 2c) and SEM-EDS analyses (Figure 3c). The latter analysis allowed us to investigate the features of the binder, characterized by a heterogeneous micritic aspect and composed of Ca, Si, Al and Mg, not homogeneously distributed in the matrix (Figure 3 a–b).
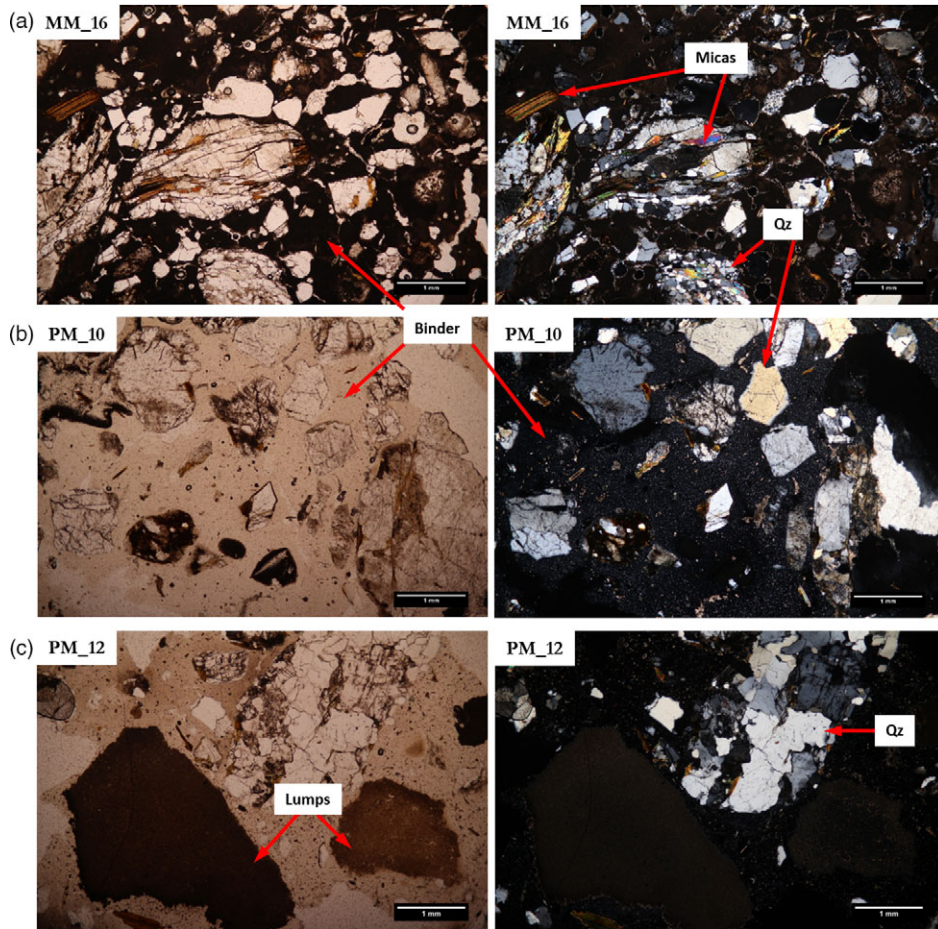
Figure 2 Transmitted light OM of 3 thin sections, plane polarized light micrographs on the left, crossed polarized light micrographs on the right: (a) and (b) MM_16 and PM_10 samples, respectively, representative of the two discriminated groups, showing the binder and aggregates, mainly quartzites (Qz) and micas; (c) PM_12 showing the presence of lime lumps.

The presence of such elements in the binder composition indicates the formation of hydrated silico-aluminate phases after reaction between the lime binder and phyllosilicates present in the aggregate fraction. Enrichments in Mg promote the formation of more compact microstructures, leading to an increase in the mechanical strength of the mortars (Dheilly et al. 1999; Diekamp et al. 2009; Bertolini et al. 2013). Identified lumps are mainly characterized by high content of Ca, and very low content of Si, Mg and Al (Figure 3c), suggesting the use of rather pure calcic binder.

The results of XRPD analyses of bulk samples in terms of quantitative mineralogical composition (wt%±Rietveld error) are reported in Table 1. Quartz, k-feldspar (microcline), plagioclase (albite) and phyllosilicates (muscovite, biotite and chlorite) are consistent with the aggregate composition. The occurrence of phyllosilicates may be also related to a silty fraction added to the lime mixture, probably related to an inaccurate purification of the aggregate prior to mortar mixing. The presence of calcite (up to 23 wt%) is attributed to a
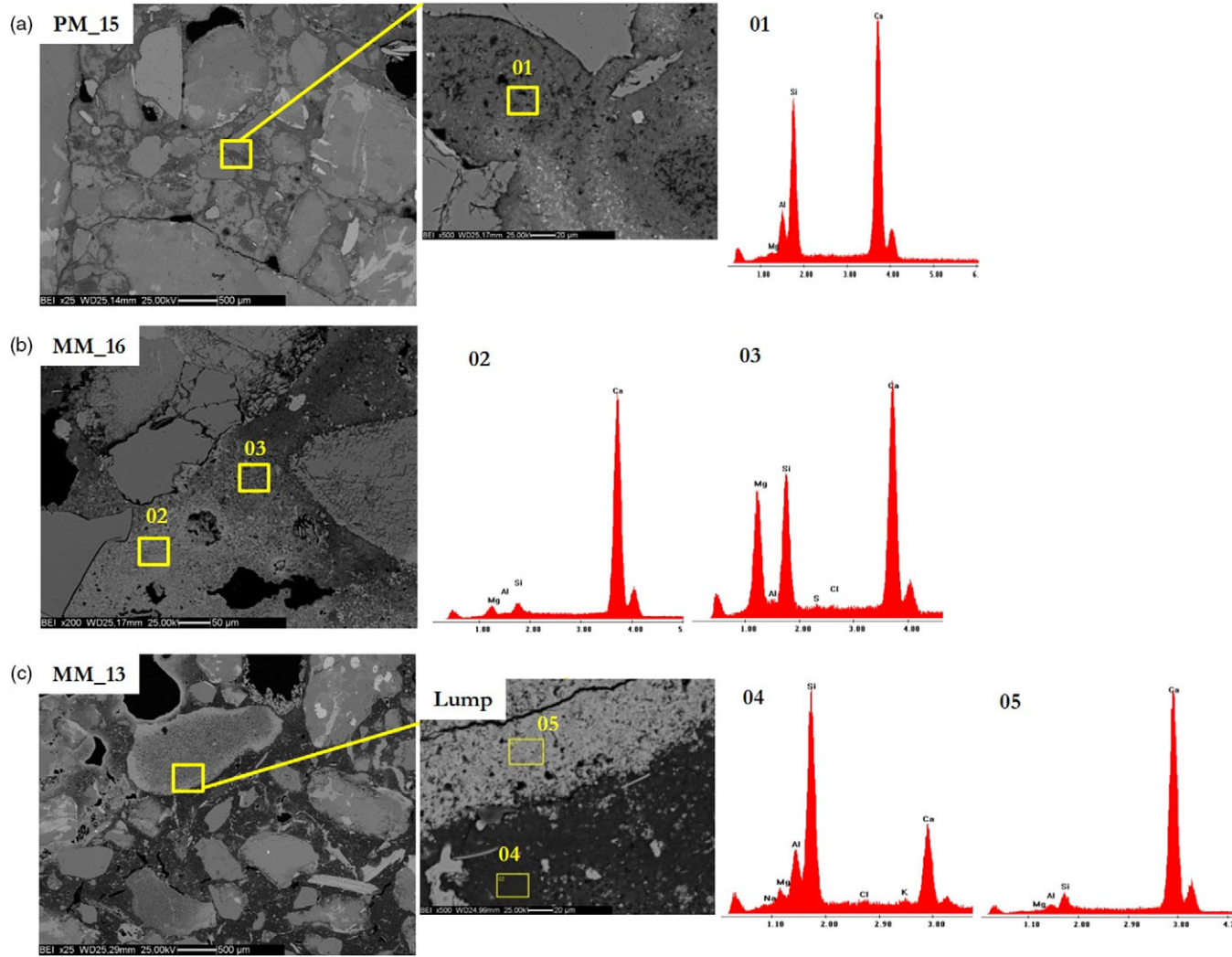
Figure 3   SEM-EDS analyses of 3 characteristic samples: (a) Sample PM_15, backscattered electron images (BSI) of the thin section and microanalyses of the matrix (01); (b) A BSI of the sample MM_16 and EDS microanalyses of the highlighted points of the heterogeneous matrix (02-04); (c) BSIs of MM_13 and EDS microanalyses of the matrix and lump.

Table 1   QPA (wt%±Rietveld error) of the analysed samples, both bulk and binder fraction (SG).

Sample code	Note	Cal	Ar	Vat	LDH	HMg	Mg	Br	Qz	Plg	K-fld	Micas	Amph	CCl	Am
PM_1	Bulk	15.2 (0.1)	0.00	0.00	1.8 (0.1)	3.7 (0.2)	0.00	0.00	22.4 (0.2)	19.4 (0.7)	7.4 (0.6)	5.6 (0.4)	0.5 (0.4)	3.4 (0.3)	20.3 (0.8)
PM_2		12.4 (0.8)	3.0 (0.2)	0.00	1.1 (0.7)	0.00	0.00	0.00	29.9 (0.2)	23.1 (0.8)	7.4 (0.5)	7.9 (0.4)	0.00	3.9 (0.3)	11.3 (0.8)
AM_3		12.6 (0.7)	0.00	0.00	1.0 (0.6)	0.00	5.8 (0.3)	0.00	33.8 (0.2)	15.6 (0.9)	7.3 (0.4)	7.2 (0.3)	0.00	3.2 (0.2)	13.6 (0.6)
PM_5		14.2 (0.8)	0.6 (0.4)	0.00	0.8 (0.4)	1.9 (0.1)	0.00	0.00	28.9 (0.1)	22.7 (0.7)	5.9 (0.3)	5.9 (0.2)	0.00	3.5 (0.2)	15.6 (0.7)
MM_6		22.6 (0.1)	0.00	0.00	0.00	0.00	0.00	0.00	26.0 (0.2)	24.3 (0.8)	3.3 (0.2)	6.0 (0.2)	0.5 (0.3)	3.4 (0.2)	13.9 (0.7)
PM_7		11.9 (0.7)	0.00	0.00	0.6 (0.3)	3.2 (0.2)	0.00	0.00	36.3 (0.2)	20.4 (0.7)	6.6 (0.4)	5.0 (0.5)	0.7 (0.5)	3.1 (0.2)	12.2 (0.7)
PM_9		5.8 (0.3)	0.00	0.00	0.00	0.00	0.00	0.00	34.3 (0.2)	33,3 (0.4)	7.1 (0.4)	3.5 (0.5)	1.2 (0.7)	3.5 (0.2)	10.8 (0.7)
PM_10		11.2 (0.6)	0.00	2.2 (0.1)	0.00	0.00	0.00	0.00	31.9 (0.2)	30.0 (0.8)	6.6 (0.3)	2.7 (0.3)	0.6 (0.3)	2.5 (0.1)	12.2 (0.6)
PM_11		19.6 (0.1)	0.00	0.6 (0.4)	0.00	0.00	0.00	0.00	27.6 (0.2)	18.3(0.6)	5.9 (0.4)	2.2 (0.6)	2.1 (0.1)	3.2 (0.2)	20.5 (0.6)
PM_12		8.6 (0.5)	0.00	0.4 (0.2)	0.00	0.00	0.00	0.00	33.0 (0.2)	18.7 (0.6)	7.2 (0.5)	4.4 (0.5)	1.8 (0.1)	2.6 (0.2)	23.3 (0.6)
MM_13		15.2 (0.9)	0.00	0.1 (0.9)	0.00	0.00	0.00	0.00	32.3 (0.2)	24.4 (0.7)	6.3 (0.4)	3.5 (0.5)	1.8 (0.1)	3.1 (0.2)	13.2 (0.7)
PM_14		11.3 (0.9)	0.00	0.3 (0.2)	0.00	0.00	0.00	0.00	34.7 (0.3)	26.9 (0.5)	6.5 (0.5)	6.5 (0.3)	3.7 (0.3)	4.9 (0.4)	5.9 (0.9)
PM_15		8.0 (0.5)	0.00	0.7 (0.4)	0.1 (0.7)	0.00	0.00	0.00	31.8 (0.2)	28.9 (0.4)	6.8 (0.4)	5.7 (0.2)	1.3 (0.8)	2.0 (0.1)	14.7 (0.7)
MM_16		15.5 (0.1)	0.00	0.00	3.7 (0.3)	3.8 (0.3)	0.00	0.00	29.1 (0.2)	15.9 (0.6)	5.5 (0.4)	4.9 (0.2)	2.1 (0.2)	5.2 (0.4)	14.3 (0.9)
PM_5	SG	25.2 (0.3)	2.4 (0.2)	0.00	17.7 (0.3)	14.6 (0.1)	0.00	0.00	0.00	0.00	0.00	0.00	0.00	0.00	40.1 (0.9)
PM_7		33.7 (0.3)	0.00	0.00	12.5 (0.3)	20.0 (0.1)	0.00	0.00	0.00	0.00	0.00	0.00	0.00	0.00	33.8 (0.7)
PM_9		15.7 (0.2)	0.00	0.00	0.3 (0.3)	0.00	0.00	0.00	0.00	0.00	0.00	3.5 (0.3)	0.00	1.1 (0.8)	79.4 (0.4)
PM_10		28.9 (0.2)	0.00	1.1 (0.1)	0.8 (0.4)	0.00	0.00	0.00	1.0 (0.7)	1.7 (0.7)	0.00	0.00	0.00	0.8 (0.4)	65.7 (0.4)
PM_12		7.6 (0.1)	0.00	0.00	2.8 (0.2)	0.00	0.00	0.00	0.00	0.00	0.00	1.4 (0.2)	0.00	5.1 (0.7)	83.1 (0.5)
PM_14		16.2 (0.2)	0.00	0.00	7.4 (0.5)	0.00	0.00	1.9 (0.2)	0.00	0.00	0.00	4.4 (0.5)	0.00	5.1 (0.5)	65.0 (0.7)
PM_15		36.6 (0.2)	0.00	0.9 (0.7)	1.2 (0.6)	0.00	0.00	0.00	0.00	0.00	0.00	2.9 (0.2)	0.00	1.3 (0.6)	57.1 (0.5)
MM_16		32.4 (0.3)	0.4 (0.3)	0.00	0.3 (0.2)	8.9 (0.8)	0.00	0.00	0.00	0.00	0.00	0.00	0.00	8.2 (0.9)	49.8 (0.7)

Cal=calcite, Ar=aragonite, Vat=vaterite, LDH=Hydrotalcite-type, HMg=hydromagnesite, Mg=magnesite, Bru=brucite, Qz=quartz, Pl=plagioclase, K-fld=K-feldspar, Micas=muscovite and biotite, Amph=amphibole, CCl=Clinochlore, Am=Amorphous phases.

partial aerial reaction of the binder fraction, since no calcite or other carbonate aggregates were identified by the petrographic analyses. The presence of phyllosilicates involves pozzolanic reactions forming silicate and aluminate hydrated compounds which are insoluble in water and therefore capable of conferring excellent resistance properties to binder materials. Relative high aliquots of amorphous phases (generally between 13 to 24 wt%) and the presence of LDH compounds (up to 3.5 wt%) indicate hydraulic interactions between lime and reactive silicate aggregates, such as Mg-rich phyllosilicates, as shown by the binder matrix elemental composition investigated by SEM-EDS results (Matschei et al. 2007). These raw materials provide Mg and Al ions in a hyper-alkaline condition, promoting the formation of LDHs during the setting and hardening process. Hydromagnesite and magnesite, identified in some of the samples, may be related to the carbonation processes of the Mg ions released during the breakdown of the Mg-rich silicates in alkaline environment.

The hydraulic reaction is confirmed also by the presence of aragonite and vaterite, detected in low amount (max 3 wt%) in most of the samples. These minerals are metastable polymorphs of calcium carbonate and may form within the mixtures due to an alteration of the C-S-H phases formed after pozzolanic reaction (Taylor 1997; Provis et al. 2015; Jackson et al. 2017) and/or, in the case of aragonite present in small amount, it may be due to the carbonation process of CaO (Toffolo and Boaretto 2014).

Fine purified binder fractions (SG) of 8 selected mortars were extracted following the procedures developed in our laboratories and XRPD analyses were carried out in order to better characterize the binder fractions (Table 1). SGs are mainly characterized by a high amount of amorphous phases (between 30 to 83 wt%), calcite (7 to 35 wt%), and LDHs (up to 17 wt%). These results denote the efficacy of the sedimentation protocol allowing to obtain a complete separation of the binder particles from the other components of the mortars. The presence of phases related to pozzolanic reactions, as hydrotalcite-like compounds, may perturb the original ^{14}C signal, therefore, a further purification process was applied.

Radiocarbon Dating

Mortars, as well as charcoal fragments (CM), have been dated to understand the construction sequence of the Cannero complex. ^{14}C dating results are summarized in Table 2 in which carbon mass (mc in mg), percent of modern carbon (pMC), radiocarbon age (BP) and calibrated age range (1 and 2σ) in cal yr AD are reported.

Before discussing the obtained dates in an archaeological context, it is interesting to note the effectiveness of the applied methodology. The OTTs correspond to the CO_2 released after the thermal treatment by the LDH contaminants and their dates are all younger except one (PM_7 sample) than the residues (RaTT) representing the purified carbonate binder, as shown in Figure 4a. This is proved in the sample MM_16, collected right above the inscription with the date 1522. The MM_16 OTT date is younger than RaTT date, which have 98.28 (0.61) and 96.70 (0.38) pMC, respectively. The latter is perfectly consistent with the inscription on the wall, as showed in the area III in Figure 4a where the graffiti date (1522) is converted in pMC (95.9 (0.2)). Similarly, both PM_10 and PM_15 show the pMC of OTTs higher than RaTTs, as reported in Table 2. These two samples were collected from the large west court and the main court of the complex, where the archaeologists had difficulties to discriminate the different structures. The

Table 2 ^{14}C dating results of charcoal fragments (CM) found in the mortar samples. reporting both the outcome of thermal treatment (OTT) and the residual after thermal treatment (RaTT) of the binder fraction of mortars dated by the AMS technique in the CIRCE laboratory in Caserta.

CIRCE code	Sample name	Area	Dated material	Fraction	mC (mg)	^{14}C (pMC)	^{14}C age (BP)	Cal AD age range (1σ)	Cal AD age range (2σ)
DSH8490	CM_4	I	Charcoal from mortar			95.93 (0.31)	333±26	AD 1495–1633	AD 1481–1641
DSH8655	PM_5	I	Binder Mortar (SG)	OTT	3.4 (0.3)	96.09 (0.37)	320±31	AD 1517–1640	AD 1482–1646
DSH8660				RaTT	2.2 (0.2)	95.21 (0.45)	394±38	AD 1445–1617	AD 1436–1633
DSH8492	CM_7	I	Charcoal from mortar			96.64 (0.48)	349±29	AD 1483–1630	AD 1460–1635
DSH8656	PM_7	I	Binder Mortar (SG)	OTT	3.9 (0.3)	93.98 (0.38)	499±33	AD 1413–1439	AD 1329–1450
DSH8661				RaTT	3.4 (0.3)	96.64 (0.48)	275±40	AD 1522–1664	AD 1485–1944
DSH8491	CM_8	I	Charcoal from mortar			95.39 (0.33)	379±28	AD 1452–1617	AD 1446–1632
DSH8657	PM_9	II	Binder Mortar (SG)	OTT	1.3 (0.2)	96.74 (0.44)	266±37	AD 1524–1796	AD 1490–1941
DSH8658	PM_10	II	Binder Mortar (SG)	OTT	2.1 (0.2)	95.60 (0.45)	361±38	AD 1464–1625	AD 1450–1635
DSH8663				RaTT	0.9 (0.2)	94.31 (0.43)	470±36	AD 1420–1448	AD 1401–1479
DSH8659	PM_12	II	Binder Mortar (SG)	OTT	0.4 (0.2)	98.85 (0.56)	93±46	AD 1694–1919	AD 1678–1940
DSH 8667	PM_14	II	Binder Mortar (SG)	OTT	0.5 (0.2)	99.61 (0.50)	32±41	AD 1699–1916	AD 1691–1925
DSH8674				RaTT	0.2 (0.2)	97.50 (0.80)	204±65	AD 1642–1903	AD 1522–1903
DSH8668	PM_15	II	Binder Mortar (SG)	OTT	1.4 (0.2)	96.81 (0.44)	260±36	AD 1526–1797	AD 1495–1939
DSH8675				RaTT	0.9 (0.2)	94.04 (0.48)	493±41	AD 1409 1444	AD 1320–1465
DSH8669	MM_16	III	Binder Mortar (SG)	OTT	2.0 (0.2)	98.28 (0.61)	139±50	AD 1676–1941	AD 1666–1950
DSH8676				RaTT	2.6 (0.2)	96.70 (0.38)	269±31	AD 1525–1791	AD 1499–1799
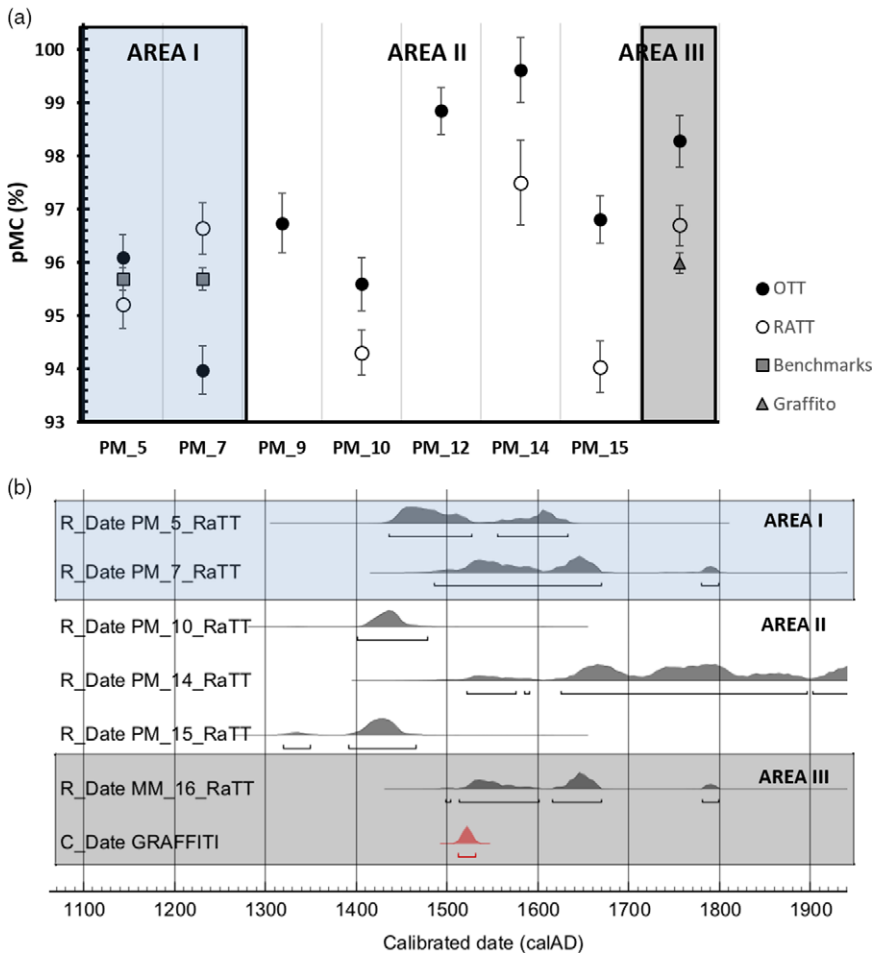
Figure 4 ^{14}C dating results: (a) Comparison between OTT and RaTT pMC ± standard errors of each SG samples and expected date converted in pMC; benchmarks refer to the weighted average of the 3 charcoals collected in the mortars of the same area and graffiti to the inscription (1522), both reported for graphical purpose. (b) Calibrated dates of the ^{14}C measurements of mortar samples (SG_RaTT) by means of OxCal 4.2 (Bronk Ramsey and Lee 2013) and IntCal 13 calibration curve (Reimer et al. 2013).

results show both the date older than 1500 (AD 1402–1477 2σ at 95.4% and AD 1391–1466 2σ at 88.1%, PM_10 and PM_15 respectively), suggesting that the structures are not linked to the building phase of Ludovico Borromeo (Figure 4b). Concerning the older date obtained from PM_7 OTT than the PM_7 RaTT, this exception may be due the features and eventual presence of contaminants of the sample itself. The mortar was sampled from the hearth at the ground floor of the area I. It was rich in carbonaceous residues and plausibly constituted by fine allochthonous sediment to the mortar, potentially containing fine and ultrafine geogenic carbonate fractions that could have backdated the sample. Radiocarbon ages of the mortars PM_5 and PM_7 (RaTTs) are compatible with those of charcoals (CM_4, CM_7 and CM_8), all collected into the residential buildings and referable to the end of the 15th century, directly connected to the Ludovico Borromeo's fortress of at the beginning of 16th century in accordance with the historical information

on the age of construction of the castle. The charcoals dates agree with each other and the mortar samples of the same area; their weighted average produces a pMC of 95.7 (0.2), used as benchmark in Figure 4a, that leads to a ^{14}C date of 354 ± 18 BP.

All the obtained data are within 2σ from the benchmarks and the graffiti date, proving the effectiveness of the procedure. In particular cases, as PM_9 and PM_12, the CO_2 extracted from the RaTTs by acid digestion, was not enough to be collected and measured by AMS due to the low amount of calcite in the samples (Table 1). Furthermore, another problematic sample was PM_14, rich in LDHs: despite being subjected to heat treatment, this was not sufficient to purify the binder, so the obtained RaTT date seems to be too young (17th–19th century).

CONCLUSIONS

The identification of the mineral phases present in the binder fraction (SG) for ^{14}C dating is crucial, yielding a preliminary understanding of the timing of the carbonation reactions and helping to decipher the complex genesis of hydraulic products in pozzolanic mortars. The obtained results show agreement among the charcoals and the mortars, confirming the archaeological expectations for the fortified complex of Cannero and adding new insights towards the archaeological interpretation. The results presented in this paper indicate the reliability of the applied procedure for chronology reconstruction and highlight the potential of both wet gravimetric separation and thermal treatment to investigate hydraulic mortars containing LDH phases.

ACKNOWLEDGMENTS

REFERENCES

Addis A, Secco M, Marzaioli F, Artioli G, Arnau AC, Passariello I, Terrasi F, Brogiolo G Pietro. 2019. Selecting the most reliable ^{14}C dating material inside mortars: The origin of the Padua Cathedral. Radiocarbon 61(2):375–393. doi: 10.1017/RDC.2018.147.

Artioli G. 2010. Scientific methods and cultural heritage. Oxford University Press.

Artioli G, Secco M, Addis A, Bellotto M. 2017. Role of hydrotalcite-type layered double hydroxides in delayed pozzolanic reactions and their bearing on mortar dating: Composition, properties, application. In: Herbert P, editor. Cementitious materials: Composition, properties, application. Berlin: Walter de Gruyter GmbH. p. 500.

Beneo E. 1961. Carta Geologica d'Italia alla scala 1:100000, foglio 16 "Cannobio", Istituto Geografico Militare, Roma.

Berger R. 1992. ^{14}C dating mortar in Ireland. Radiocarbon 34(3):880–889.

Bertolini L, Carsana M, Gastaldi M, Lollini F, Redaelli E. 2013. Binder characterisation of mortars used at different ages in the San Lorenzo church in Milan. Mater Charact. 80:9–20. doi: 10.1016/j.matchar.2013.03.008.

Bhattacharjya D, Selvamani T, Mukhopadhyay I. 2012. Thermal decomposition of hydromagnesite effect of morphology on the kinetic parameters. Journal of Thermal Analysis and Calorimetry 107(2):439–45.

Bottacchi MB, Mancini C. 2000. Storia e fantasia ai castelli di Cannero. Italy: Alberti Libraio Editore.

Brandon CJ, Hohlfelder RL, Jackson MD, Oleson JP. 2014. Building for eternity: The history and technology of roman concrete engineering

in the sea. Oleson JP, editor. Oxford: Oxbow Books.

Bronk Ramsey C, Lee S. 2013. Recent and planned developments of the program oxcal. Radiocarbon 55(2):720–731.

Conterosito E, Gianotti V, Palin L, Boccaleri E, Viterbo D, Milanesio M. 2018. Facile preparation methods of hydrotalcite layered materials and their structural characterization by combined techniques. Inorganica Chim Acta. 470:36–50. doi: 10.1016/j.ica.2017.08.007.

Delibrias G, Labeyrie J. 1964. Dating of old mortars by the carbon-14 method. Nature:201.

Dheilly RM, Bouguerra A, Beaudoin B, Tudo J, Queneudec M. 1999. Hydromagnesite development in magnesian lime mortars. Materials Science Engineering A 268(1–2):127–131. doi: 10.1016/S0921-5093(99)00085-4.

Diekamp A, Konzett J, Mirwald PW, Tyrol S. 2009. Magnesian lime mortars – identification of magnesium-phases. In: 12th Euroseminar on Microscopy Applied to Building Materials. p. 309–318.

Frigerio P, Pisoni PG. 2006. Fratelli della Malpaga: storia dei Mazzarditi. Alberti, editor.

Gualtieri AF. 2000. Accuracy of XRPD QPA using the combined Rietveld–RIR method. Journal of Applied Crystallography 33(2):267–278.

Gualtieri AF, Gatta GD, Arletti R, Artioli G, Ballirano P, Cruciani G, Guagliardi A, Malferrari D, Masciocchi N, Scardi P. 2019. Quantitative phase analysis using the Rietveld method: towards a procedure for checking the reliability and quality of the results. Periodico di Mineralogia 88:147–151. doi: 10.2451/2019PM870.

Hajdas I, Lindroos A, Heinemeier J, Ringbom Å, Marzaioli F, Terrasi F, Passariello I, Capano M, Artioli G, Addis A, et al. 2017. Preparation and dating of Mortar Samples-Mortar Dating Inter-Comparison Study (MODIS). Radiocarbon 59(6):1845–1858. doi: 10.1017/RDC.2017.112.

Heinemeier J, Ringbom Å, Lindroos A, Sveinbjörnsdóttir ÁE. 2010. Successful AMS ^{14}C dating of non-hydraulic lime mortars from the medieval churches of the Åland Islands, Finland. Radiocarbon 52(1):171–204.

Hollingbery LA, Hull TR. 2010. The thermal decomposition of huntite and hydromagnesite—a review. Thermochimica Acta 509(1–2):1–11.

Ishihara S, Sahoo P, Deguchi K, Ohki S, Tansho M, Shimizu T, Labuta J, Hill JP, Ariga K, Watanabe K, et al. 2013. Dynamic breathing of CO_2 by hydrotalcite. Journal of the American Chemical Society 135(48):18040–18043. doi: 10.1021/ja4099752.

Jackson MD, Mulcahy SR, Chen H, Li Y, Li Q, Cappelletti P, Wenk HR. 2017. Phillipsite and Al-tobermorite mineral cements produced through low-temperature water-rock reactions in Roman

marine concrete. Am Mineral. 102(7):1435–1450. doi: 10.2138/am-2017-5993CCBY.

Lindroos A, Heinemeier J, Ringbom Å, Braskèn M, Sveinbjörnsdóttir Á. 2007. Mortar dating using AMS ^{14}C and sequential dissolution: examples from medieval, non-hydraulic lime mortars from the Aland Island, SW Finland. Radiocarbon 49(1):47–67.

Lose F, Lose C. 1818. Viaggio pittorico e storico ai tre laghi Maggiore, di Lugano e Como. Milano: Francesco Bernuca.

Madsen IC, Scarlett NVY. 2008. Quantitative Phase analysis. In: Dinnebier RE, Billinge SJL, editors. Powder diffraction: Theory and practice. Cambridge: RSC Publishing. p. 298–331.

Marzaioli F, Borriello G, Passariello I, Lubritto C, De Cesare N, D'Onofrio A, Terrasi F. 2008. Zinc reduction as an alternative method for AMS radiocarbon dating : Process optimization at CIRCE. Radiocarbon 50(1):139–149.

Marzaioli F, Lubritto C, Nonni S, Passariello I, Capano M, Ottaviano L, Terrasi F. 2014. Characterisation of a new protocol for mortar dating: ^{14}C evidences. Open Journal of Archaeometry 2(2):55–59.

Marzaioli F, Lubritto C, Nonni S, Passariello I, Capano M, Terrasi F. 2011. Mortar radiocarbon dating: Preliminary accuracy evaluation of a novel methodology. Anal Chem. 83(6):2038–2045. doi: 10.1021/ac1027462.

Matschei T, Lothenbach B, Glasser FP. 2007. The AFm phase in Portland cement. Cement and Concrete Research 37(2):118–130. doi: 10.1016/j.cemconres.2006.10.010.

Michalska D, Czernik J. 2015. Carbonates in leaching reactions in context of ^{14}C dating. Nuclear Instruments and Methods in Physics Research B 361:431–439. doi: 10.1016/j.nimb.2015.08.033.

Miriello D, Barca D, Bloise A, Ciarallo A, Crisci GM, De Rose T, Gattuso C, Gazineo F, La Russa MF. 2010. Characterisation of archaeological mortars from Pompeii (Campania, Italy) and identification of construction phases by compositional data analysis. Journal of Archaeological Science 37(9):2207–2223. doi: 10.1016/j.jas.2010.03.019.

Mishra G, Dash B, Pandey S. 2018. Layered double hydroxides: A brief review from fundamentals to application as evolving biomaterials. Applied Clay Science 153(October 2017):172–186. doi: 10.1016/j.clay.2017.12.021.

Nawrocka D, Michniewicz J, Pawlyta J. 2005. Application of radiocarbon method for dating of lime mortars. Geochronometria 24:109–115.

Nonni S, Marzaioli F, Secco M, Passariello I, Capano M, Lubritto C, Mignardi S, Tonghini C, Terrasi F. 2017. ^{14}C mortar dating: The case of the Medieval Shayzar Citadel, Syria. Radiocarbon 55(2):514–525. doi: 10.1017/s0033822200057647.

Passariello I, Marzaioli F, Lubritto C, Rubino M, D'Onofrio A, De Cesare N, Rogalla D, Sabbarese C, Palmieri A, Borriello G, et al. 2007. Radiocarbon sample preparation at the CIRCE AMS laboratory in Caserta, Italy. Radiocarbon 49(02):225–232. doi: 10.1017/s0033822200042156.

Pérez-Ramírez J, Abelló S. 2006. Thermal decomposition of hydrotalcite-like compounds studied by a novel Tapered Element Oscillating Microbalance (TEOM). Comparison with TGA and DTA. Thermochimica Acta 444(1):75–82.

Pisoni CA. 2003. Pro arce della Vittaliana. Excursus storico per una fortalicium di breve vita, rudere di grand fascino, in Cannero Riviera tra lago e monti. Storia d'una terra e d'una parrocchia. Alberti editore V, editor.

Ponce-Antón G, Ortega L, Zuluaga M, Alonso-Olazabal A, Solaun J. 2018. Hydrotalcite and Hydrocalumite in mortar binders from the Medieval Castle of Portilla (Álava, North Spain): Accurate mineralogical control to achieve more reliable chronological ages. Minerals 8(8):326. doi: 10.3390/min8080326.

Provis JL, Palomo A, Shi C. 2015. Advances in understanding alkali-activated materials. Cement and Concrete Research 78:110–125. doi: 10.1016/j.cemconres.2015.04.013.

Reimer PJ, Bard E, Bayliss A, Beck JW, Blackwell PG, Bronk Ramsey C, Buck CE, Cheng H, Edwards RL, Friedrich M, et al. 2013. IntCal13 and Marine13 radiocarbon age calibration curves 0–50,000 years cal BP. Radiocarbon 46(1):1111–1150. doi: 10.2458/azu_js_rc.46.4183.

Rietveld HM. 1969. A profile refinement method for nuclear and magnetic structures. Journal of Applied Crystallography 2:65–71. doi: 10.1107/s0021889869006558.

Roelofs JCAA, van Bokhoven JA, van Dillen AJ, Geus JW, de Jong KP. 2002. The thermal decomposition of Mg-Al hydrotalcites: effects of interlayer anions and characteristics of the final structure. Chem–A Eur J. 8(24):5571–5579. doi: 10.1002/1521-3765(20021216)8:24<5571::aid-chem5571>3.0.co;2-r.

Secco M, Dilaria S, Addis A, Bonetto J, Artioli G, Salvadori M. 2018. The evolution of the Vitruvian recipes over 500 years of floor-making techniques: the case studies of the Domus delle Bestie Ferite and the Domus di Tito Macro (Aquileia, Italy). Archaeometry 60(2):185–206. doi: 10.1111/arcm.12305.

Sonninen E, Jungner H. 2001. An improvement in preparation of mortar for radiocarbon dating. Radiocarbon 43(2):271–273.

Stanimirova Ts, Vergilov I, Kirov G, Petrova N. 1999. Thermal decomposition products of hydrotalcite-like compounds: low-temperature metaphases. Journal of Materials Science 34(17):4153–61.

Van Strydonck M. 2016. Radiocarbon dating of lime mortars: a historic overview. In: 4th Historic Mortars Conference HMC2016. p. 648–655.

Stuiver M, Polach H. 1977. Discussion: Reporting of ^{14}C data. Radiocarbon 19(3):355–366.

Taylor HFW. 1997. Cement chemistry. 2nd ed. London: Thomas Telford Publishing.

Terrasi F, De Cesare N, D'Onofrio A, Passariello I, Rogalla D, Sabbarese C, Borriello G, Casa G, Palmieri A. 2008. High precision ^{14}C AMS at CIRCE. Nuclear Instruments and Methods in Physics Research B 266(10):2221–2224.

Tian J, Guo Q, Tian J, Guo Q. 2014. Thermal decomposition of hydrocalumite over a temperature range of 400-1500°C and its structure reconstruction in water. Journal of Chemistry. doi: 10.1155/2014/454098, 10.1155/2014/454098.

Toffolo MB, Boaretto E. 2014. Nucleation of aragonite upon carbonation of calcium oxide and calcium hydroxide at ambient temperatures and pressures: a new indicator of fire-related human activities. Journal of Archaeological Science 49:237–248. doi: 10.1016/j.jas.2014.05.020.

Trindade MJ, Dias MI, Coroado J, Rocha F. 2009. Mineralogical transformations of calcareous rich clays with firing: a comparative study between calcite and dolomite rich clays from Algarve, Portugal. Applied Clay Science 42(3–4):345–55.

Vieille L, Rousselot I, Leroux F, Besse JP, Taviot-Guého C. 2003. Hydrocalumite and its polymer derivatives. 1. Reversible thermal behavior of Friedel's Salt: a direct observation by means of high-temperature in situ powder X-ray diffraction. Chemistry of Materials 15(23):4361–68.